Available online at www.sciencedirect.com
SCIENCE DIRECT®
Organic Electronics 6 (2005) 3–9
Organic Electronics
www.elsevier.com/locate/orgel

Theoretical analysis on light-extraction efficiency of organic light-emitting diodes using FDTD and mode-expansion methods

Alongkarn Chutinan *, Kuniaki Ishihara, Takashi Asano, Masayuki Fujita, Susumu Noda *

Department of Electronic Science and Engineering, Kyoto University, Kyotodaigaku-katsura, Nishikyo-ku, Kyoto 615-8510, Japan
CREST, Japan Science and Technology Corporation, Japan

Received 5 February 2004; received in revised form 25 November 2004; accepted 4 December 2004
Available online 21 December 2004

Abstract

We report a theoretical analysis on light-extraction efficiency of the organic light-emitting diodes. We utilize both a numerical method such as the finite-difference time-domain method and an analytic method such as the mode-expansion method. The results of both methods are compared to confirm the accuracy of the results. It is found that even though the refractive index contrast between the indium-tin-oxide (ITO) anode and the glass substrate is as small as 0.5, more than 40% of emitted light power is trapped in the ITO layer.

PACS: 78.20.Bh
Keywords: Organic light-emitting diode; FDTD; Mode-expansion method

1. Introduction

Organic light-emitting diodes (OLEDs) have attracted much attention due to their strong potentials for flat panel display applications. However, the low light-extraction efficiency of OLEDs still remains an important issue and poses a significant challenge for researchers to develop schemes that improve the light coupling efficiency [1]. In order to do so, it is necessary to fully understand the coupling of emitted light to the surrounding materials and free space. The issue regarding the light-extraction efficiency of the OLEDs has been investigated theoretically or experimentally in

* Corresponding authors. Tel.: +416 978 5207; fax: +416 978 2537 (A. Chutinan); tel.: +81 75 383 2315/2319; fax: +81 75 383 2317/2320 (S. Noda).
E-mail addresses: chutinan@physics.utoronto.ca (A. Chutinan), snoda@kuee.kyoto-u.ac.jp (S. Noda).

1566-1199/$ - see front matter
doi:10.1016/j.orgel.2004.12.001

various articles [2–6]. In the theoretical analyses reported, a number of models ranging from the classical ray optics [2] to the combined classical and quantum mechanical microcavity [3] are utilized. However, a non-trivial discrepancy can be seen among different articles. In this paper, we report a light-extraction efficiency analysis of the OLED where both the numerical method such as the finite-difference time-domain (FDTD) method and the analytic method such as the mode-expansion method are used. The results of FDTD are compared with those of the mode-expansion method to confirm the accuracy of the results.

2. Calculation of light-extraction efficiency by 3D FDTD

Fig. 1 shows a schematic of the OLED structure studied here. The structure consists of a metal cathode, a tris-(9-hydroxyquinoline) aluminum (Alq_3, refractive index $n_1 = 1.7$), a poly-(*N*-vinylcarbazole) (PVK, $n_2 = 1.67$), an indium-tin-oxide (ITO, $n_3 = 2.0$) anode and a glass substrate ($n_4 = 1.5$). Here, we assumed that the light is emitted from the excitons, which are created at the interface of the Alq_3 and PVK layers. The emitted light can be categorized into three modes: the waveguide modes that are trapped inside the organic and ITO layer, the glass modes that escape the ITO layer but are trapped in the glass substrate by total internal reflection at the interface of glass and air, and the air modes that escape the glass substrate to air.

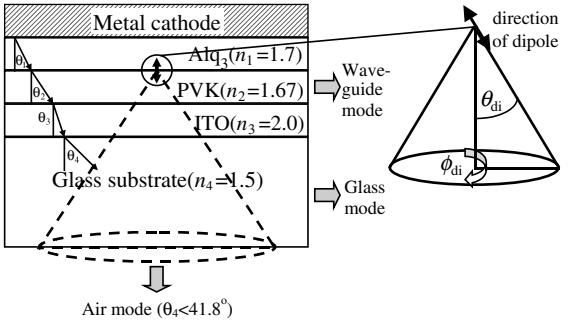

Fig. 1. Schematic depicting the OLED structure and computational model. The structure consists of four layers, i.e., Alq_3, PVK, ITO and the glass substrate. The dipole is placed at the Alq_3/PVK interface and can align in arbitrary direction described by angles ϕ_{di} and θ_{di}.

First, we explain the calculation by the three-dimensional (3D) FDTD method [7]. The above-described OLED structure is modeled inside the FDTD computational domain. The metal cathode is modeled as a perfect electric conductor and the absorption loss is not considered here. The substrate is modeled as a very thick layer of glass and is terminated by the Mur's secondary absorbing boundary condition [8], which allows electromagnetic waves to propagate out of the computational domain without being reflected back into the computational domain. This is equivalent to that the glass substrate is assumed to be infinitely thick. The spatial and temporal resolution of our FDTD calculation are 10 nm and 0.33 fs, respectively. The size of computational domain is $9800 \times 9800 \times 1000$ nm, where the last dimension refers to the direction perpendicular to the OLED layers. As shown in Fig. 1, the power of the waveguide mode is determined by simply calculating the power that flows along the Alq_3/PVK/ITO waveguide. The power transmission from glass to air is treated by ray optics [4], i.e., the light that propagates inside the glass substrate with an angle less than the critical angle of glass/air (41.8°) is considered as the air mode and the light that propagates inside the glass substrate with an angle larger than 41.8° is considered as the glass mode. A dipole is placed at the Alq_3/PVK interface and excited by a continuous wave with the wavelength $\lambda = 524$ nm. The emitted powers are obtained after the FDTD simulations have reached steady states. In our calculations, 7000 time steps were iterated. Since the direction of dipole can be arbitrary, the results must be averaged over all dipole directions. This can be expressed by the following equation:

$$\bar{p} = \int_0^{\pi/2}\int_0^{2\pi} p(\theta_{di},\phi_{di})\sin(\theta_{di})\mathrm{d}\theta_{di}\,\mathrm{d}\phi_{di} \Big/ \int_0^{\pi/2}\int_0^{2\pi} \sin(\theta_{di})\mathrm{d}\theta_{di}\,\mathrm{d}\phi_{di}, \quad (1)$$

where $p(\theta_{di},\phi_{di})$ is the power of the waveguide mode, the glass mode, or the air mode as a function of the dipole direction θ_{di} and ϕ_{di}.

Since the OLED structure is uniform in the in-plane direction, $p(\theta_{di}, \phi_{di})$ is uniform along the angle ϕ_{di} or $p(\theta_{di}, \phi_{di}) = p(\theta_{di})$. Thus, the averaging becomes only for the θ_{di} direction. We calculate by 3D FDTD the dipole power for each mode for various θ_{di} and find that the power $p(\theta_{di})$ can be perfectly described by the equation

$$p(\theta_{di}) = p(0^\circ)\cos^2(\theta_{di}) + p(90^\circ)\sin^2(\theta_{di}). \quad (2)$$

This agrees well with the theoretical prediction by the mode-expansion method. By substituting Eq. (2) into Eq. (1), we finally obtain

$$\bar{p} = \frac{1}{3}p(0^\circ) + \frac{2}{3}p(90^\circ). \quad (3)$$

Eq. (3) implies that we only need to calculate for two different cases, $\theta_{di} = 0^\circ$ and $\theta_{di} = 90^\circ$, to obtain the average powers. We calculate the power of the waveguide mode, glass mode and air mode by FDTD for the following cases: the thickness of Alq_3 and PVK layers is 80, 40 nm, respectively, and the thickness of the ITO layer is varied from 10 to 300 nm. The results are shown by circles in Fig. 2. Fig. 2 shows the ratio of the emission rate of each mode to the total emission rate. Note that the absolute values of the total emission rates vary among the different structural parameters. We also calculate the emission rate for the case that the thickness of PVK layer is 40 nm, the thickness of the ITO layer is 150 nm, and the thickness of Alq_3 layer is varied from 10 to 300 nm. The results are shown in Fig. 3.

We note here that in the FDTD calculation, it was difficult to separate the radiation modes with radiation angle θ_{rad} near 90° from the waveguide modes since both propagate along the same direction. We have used a large computational domain to separate the radiation modes with $\theta_{rad} <\sim 80^\circ$ from the waveguide modes. This is adequate for most of the cases where the peaks in radiation patterns fall at the angle smaller than 80°. However, at some structural parameters where the radiation mode is emitted at the angle near 90°, non-negligible errors can occur. To illustrate this point, we show in Fig. 4(a) and (b) the electric field patterns emitted from the dipole for the different cases, $\theta_{di} = 0^\circ$ and $\theta_{di} = 90^\circ$, respectively. The thickness of Alq_3 layer, PVK layer and ITO layer are 80, 40 and 150, respectively. In both Fig. 4(a) and (b), only the components parallel to the dipole are shown. That is, in Fig. 4(a), only the components of electric field that are perpendicular to the OLED layer are shown. In Fig. 4(b) only the parallel components are shown. This is justified since those components shown are the strongest components in each case. As clearly visible, for $\theta_{di} = 0^\circ$, the emitted power mostly couples to the

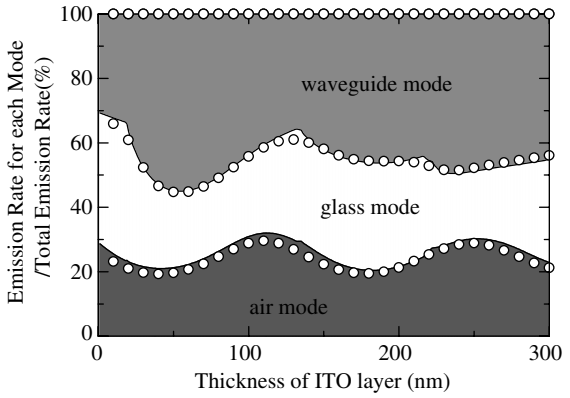

Fig. 2. Ratio of the emission rate of air modes, glass modes, and waveguide modes to the total emission rate as a function of the thickness of ITO layer. The thickness of the Alq_3 and PVK layer is 80 and 40 nm, respectively. The solid lines and circles are calculated by the mode-expansion method and the FDTD, respectively.

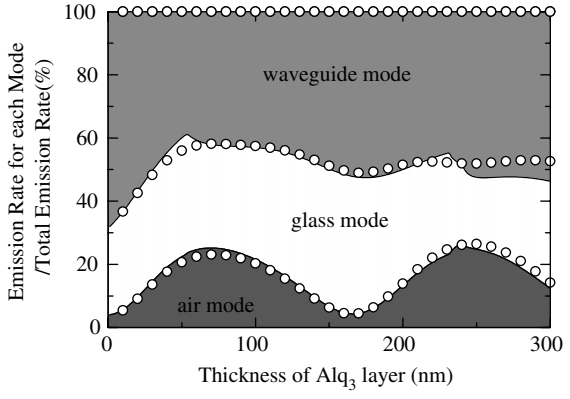

Fig. 3. Ratio of the emission rate of air modes, glass modes, and waveguide modes to the total emission rate as a function of the thickness of Alq_3 layer. The thickness of the PVK and ITO layer is 40 and 150 nm, respectively. The solid lines and circles are calculated by the mode-expansion method and the FDTD, respectively.

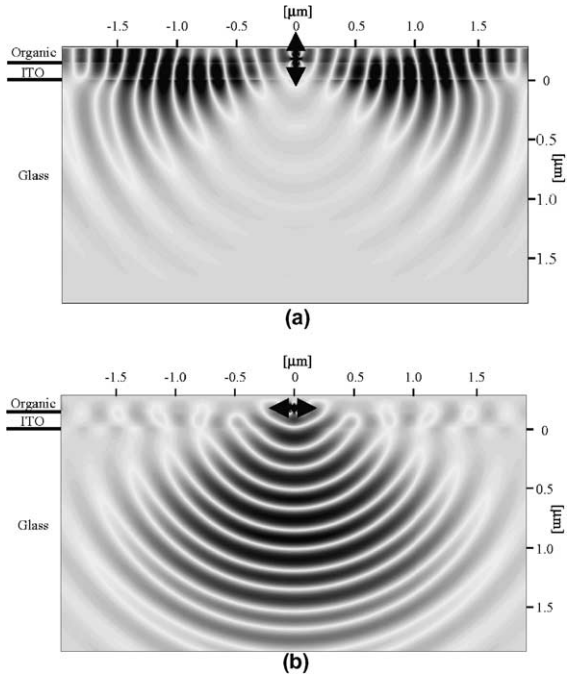

Fig. 4. Electric field patterns emitted from dipoles with different orientations. (a) $\theta_{di} = 0°$, only the components of electric field that are perpendicular to the OLED layer are shown. (b) $\theta_{di} = 90°$, only the parallel components are shown. The thickness of Alq_3 layer, PVK layer and ITO layer are 80, 40 and 150, respectively. The arrows show the direction of dipole.

waveguide mode and partially couples to the radiation modes with large radiation angles. It is especially difficult in these cases to accurately separate the waveguide modes from the radiation modes. In contrast, for $\theta_{di} = 90°$, the coupling of the emitted power to the waveguide modes and the radiation modes with large radiation angles is insignificant. Thus, the power emitted in the radiation can be determined more accurately. This will be discussed again in the next section from the mode-expansion method point of view. It is expected that separation of the radiation modes and waveguide modes by spatial filtering would improve the accuracy for FDTD.

3. Mode-expansion method

We describe the mode-expansion method for our OLED structure. The power emitted into each mode or the spontaneous emission rate for each mode γ is given by

$$\gamma = \gamma_0 \cdot \frac{3\pi^2\omega_0}{k^3} \cdot \sum_{\mu} |\hat{\mathbf{d}} \cdot \vec{\mathbf{E}}_{\mu}(\vec{\mathbf{x}}')|^2 \delta(\omega_{\mu} - \omega_0), \tag{4}$$

where γ_0 is the spontaneous emission rate in free space, $\hat{\mathbf{d}}$ is the dipole moment, $\vec{\mathbf{E}}_{\mu}(\vec{\mathbf{x}}')$ is the normalized electric field at the position of dipole, ω_0 is the angular frequency of dipole, k is the wave vector and $\sum_{\mu}$ is the summation over all wave vectors for each mode [9].

The normalization equation for electric field is given as

$$\int \varepsilon(\vec{\mathbf{x}})\vec{\mathbf{E}}^*_{\nu}(\vec{\mathbf{x}}) \cdot \vec{\mathbf{E}}_{\mu}(\vec{\mathbf{x}}) \mathrm{d}\mathbf{r} = \delta_{\mu\nu}. \tag{5}$$

The summation over all wave vectors leads to the term of density of state $\rho(\omega)$. Therefore, Eq. (4) can be rewritten as

$$\gamma = \gamma_0 \cdot \frac{3\pi^2\omega_0}{k^3} \cdot \int |\hat{\mathbf{d}} \cdot \vec{\mathbf{E}}_{\mu}(\vec{\mathbf{x}}')|^2 \delta(\omega_{\mu} - \omega_0)\rho(\omega)\mathrm{d}\omega. \tag{6}$$

First, we consider the radiation modes. The radiation eigenmodes can be described as a function of an incident angle θ for a layered structure. The density of state is also a function of θ and can be written as $\rho = \sin(\theta)$. Here, as the same as FDTD, we also consider that the glass substrate is infinitely thick. Thus, the radiation mode here refers to the mode that propagates inside the glass substrate. This is equivalent to the sum of glass modes and air modes. We use the transfer matrix formalism to solve for the eigenmodes. For S-polarized plane waves incident on an m-layers structure with an incident angle θ_m, the electric field inside each layer can be described as follows:

$$\mathbf{E}_i = (0, 0, E_{zi}), \quad i = 1 \ldots m, \tag{7}$$

where the subscript i describe the ith layer (see Fig. 1).

$$E_{zi}(y) = A_i \exp\{-j\kappa_i(y - y_i)\} + B_i \exp\{j\kappa_i(y - y_i)\}, \tag{8}$$

$$\kappa_i = k_0 n_i \cos(\theta_i), \quad n_i \sin(\theta_i) = n_m \sin(\theta_m). \tag{9}$$

Assuming $A_1 = 1$, the perfect electric conductor condition at the cathode surface gives $B_1 = -A_1 = -1$. By using Eqs. (7)–(9) and considering the continuity of the field at each interface, the coefficient for the glass layer (A_4) can be easily found. We let $U_S = |A_4|$.

Next, we consider coupling between the S-polarized waves and a dipole. It is found that the S-polarized waves couple to the 90° dipole but not the 0° dipole. Following Eq. (6) in [10] and using Eq. (6) in this paper, the emission rate of the 90° dipole to the S-polarized radiation mode can be written as

$$\begin{aligned}\gamma_{90S} &= \frac{3\pi^2}{4\pi^3}\gamma_0 \cdot \int_0^{2\pi} \sin(\phi)^2 \,\mathrm{d}\phi \\ &\quad \times \int_{-\pi/2}^{\pi/2} \sin^2(k_0 \cdot n_1 \cdot \cos(\theta_1) \cdot \mathrm{dp}) \\ &\quad \Big/ (n_4^2 \cdot U_S^2(\theta_4)) \cdot n_4^3 \cdot \sin(\theta_4)\mathrm{d}\theta_4 \\ &= \frac{3}{2}\gamma_0 \int_0^{\pi/2} \sin^2(k_0 \cdot n_1 \cdot \cos(\theta_1) \cdot \mathrm{dp}) \\ &\quad \Big/ (n_4^2 \cdot U_S^2(\theta_4)) \cdot n_4^3 \cdot \sin(\theta_4)\mathrm{d}\theta_4, \end{aligned} \tag{10}$$

where dp is the dipole position (within the Alq_3 layer) and the term $n_4^3 \cdot \sin(\theta_4)$ corresponds to the density of state for bulk glass. The emission rate into the air mode and the glass mode can be calculated by simply changing the range of integration to (0–41.8°) and (41.8–90°), respectively.

For P-polarized waves, it is found that they couple to both 0° dipole and 90° dipole. Again, following Eq. (7) in [10], the emission rate into P-polarized modes for the 90° dipole is

$$\begin{aligned}\gamma_{90P} &= \frac{3\pi^2}{4\pi^3}\gamma_0 \cdot \int_0^{2\pi} \cos(\phi)^2 \,\mathrm{d}\phi \\ &\quad \times \int_{-\pi/2}^{\pi/2} \sin^2(k_0 \cdot n_1 \cdot \cos(\theta_1) \cdot \mathrm{dp}) \\ &\quad \Big/ (n_1^2 \cdot U_P(\theta_4)^2) \cdot \cos^2(\theta_1) \cdot n_4^3 \cdot \sin(\theta_4)\mathrm{d}\theta_4 \\ &= \frac{3}{2}\gamma_0 \int_0^{\pi/2} \sin^2(k_0 \cdot n_1 \cdot \cos(\theta_1) \cdot \mathrm{dp}) \\ &\quad \Big/ (n_1^2 \cdot U_P(\theta_4)^2) \cdot \cos^2(\theta_1) \cdot n_4^3 \cdot \sin(\theta_4)\mathrm{d}\theta_4, \end{aligned} \tag{11}$$

where U_P is $|A_4|$ for the case of P-polarized waves. Similarly, following Eq. (11) in [10], the emission rate into P-polarized modes for the 0° dipole is

$$\begin{aligned}\gamma_{0P} &= \frac{3\pi^2}{4\pi^3}\gamma_0 \cdot \int_0^{2\pi} \mathrm{d}\phi \\ &\quad \times \int_{-\pi/2}^{\pi/2} \cos^2(k_0 \cdot n_1 \cdot \cos(\theta_1) \cdot \mathrm{dp}) \\ &\quad \Big/ \left(n_1^2 \cdot U_P(\theta_4)^2\right) \cdot \sin^2(\theta_1) \cdot n_4^3 \cdot \sin(\theta_4)\mathrm{d}\theta_4 \\ &= 3\gamma_0 \int_0^{\pi/2} \cos^2(k_0 \cdot n_1 \cdot \cos(\theta_1) \cdot \mathrm{dp}) \\ &\quad \Big/ \left(n_1^2 \cdot U_P(\theta_4)^2\right) \cdot \sin^2(\theta_1) \cdot n_4^3 \cdot \sin(\theta_4)\mathrm{d}\theta_4. \end{aligned} \tag{12}$$

The average emission rate for the radiation mode can be found using Eq. (3) as

$$\bar{\gamma}_{rad} = \frac{1}{3}\gamma_{0P} + \frac{2}{3}(\gamma_{90P} + \gamma_{90S}). \tag{13}$$

Second, we consider the waveguide mode. The waveguide eigenmodes are also calculated by the transfer matrix formalism. For the case of the waveguide mode, the density of state becomes a function of the phase index and group index of the waveguide mode. Using Eq. (6), we obtain the emission rate for the 0° dipole, which couples only to the TM waveguide modes.

$$\begin{aligned}\gamma_{WG0} &= \gamma_0 \cdot \frac{3}{4} \cdot \lambda \\ &\quad \times \left\{ \sum_m n_{phase}^{TM}(m) \cdot n_{group}^{TM}(m) \cdot |\vec{\mathbf{E}}_{ym}(\vec{\mathbf{x}}')|^2 \right\}, \end{aligned} \tag{14}$$

where m describes the mth order TM mode, n_{phase}^{TM} and n_{group}^{TM} are the phase index and the group index of the TM waveguide mode, respectively. Similarly, for the 90° dipole, which couples to both the TM and TE modes, the emission rate can be found as follows:

$$\begin{aligned}\gamma_{WG90} &= \gamma_0 \cdot \frac{3}{8} \cdot \lambda \\ &\quad \times \left\{ \sum_m n_{phase}^{TM}(m) \cdot n_{group}^{TM}(m) \cdot \left|\vec{\mathbf{E}}_{xm}(\vec{\mathbf{x}}')\right|^2 \right. \\ &\quad \left. + \sum_l n_{phase}^{TE}(l) \cdot n_{group}^{TE}(l) \cdot \left|\vec{\mathbf{E}}_{zl}(\vec{\mathbf{x}}')\right|^2 \right\}, \end{aligned} \tag{15}$$

where l describe the lth order TE mode, $n_{\text{phase}}^{\text{TE}}$ and $n_{\text{group}}^{\text{TE}}$ are the phase index and the group index of the TE waveguide mode, respectively.

The results for the mode-expansion mode are shown by the solid line in Fig. 2 and 3. An excellent agreement between FDTD and the mode-expansion method can be seen in both figures. Thus, the accuracy of our calculation is confirmed.

We can see in both Figs. 2 and 3 that the emission rate into the waveguide modes change abruptly at some positions as we increase the thickness of the ITO layer or the Alq_3 layer. These correspond to the change in the number of waveguide modes as the thickness of the ITO or Alq_3 layers increases. For example, in Fig. 2, the 1st order TE mode starts to appear at ITO thickness = 20 nm and the 2nd order TM mode appears at ITO thickness = 136 nm. Similarly, in Fig. 3, the 2nd order TE mode starts to appear at Alq_3 thickness = 56 nm and the 2nd order TM mode appears at Alq_3 thickness = 241 nm. In total, we may conclude that ~25% of light emitted can escape to air, ~32% is trapped in the glass substrate, and ~ 43% is trapped in the Alq_3/PVK/ITO layer.

The mode-expansion method provides detailed descriptions of light emission from the OLED, for example, the radiation pattern. We show in Fig. 5 the modal strength (intensity) as a function of propagation angle in the glass substrate for two cases with different thickness of the ITO layer. The thickness of the Alq_3 and PVK is 80 and 40 nm, respectively. The solid and dashed lines show the modal strength of the S-polarized and the P-polarized mode, respectively. First, Fig. 5(a) shows the modal strength for the case that the ITO layer is 50 nm. Fig. 5(b) show the same plot for ITO layer = 130 nm. It is seen that while the modal strength in Fig. 5(a) shows only small values for the large angle (>80°), the modal strength for the P-pol with a large angle in Fig. 5(b) is non-negligible. These values become even more significant when we calculate the emission rate, which is the integral of the modal strength multiplied by the density of state $\sin(\theta)$ over the angle θ. These emitted powers at the large angle must be measured correctly. However, as discussed in the previous section, there is difficulty in distinguishing the radiation mode with a large angle from the waveguide mode in the calculation by FDTD and this leads to non-negligible errors in the FDTD results. In contrast, for the case in Fig. 5(a), the above-described problem in FDTD results in only negligible errors. This explains why the FDTD results are slightly different from those of the mode-expansion method at some particular structural parameters. Note that the emission rate for the air mode is not affected by the above argument since the air mode contains only the mode with angle <41.8°. The small discrepancy between the FDTD and the mode-expansion method for the air mode may

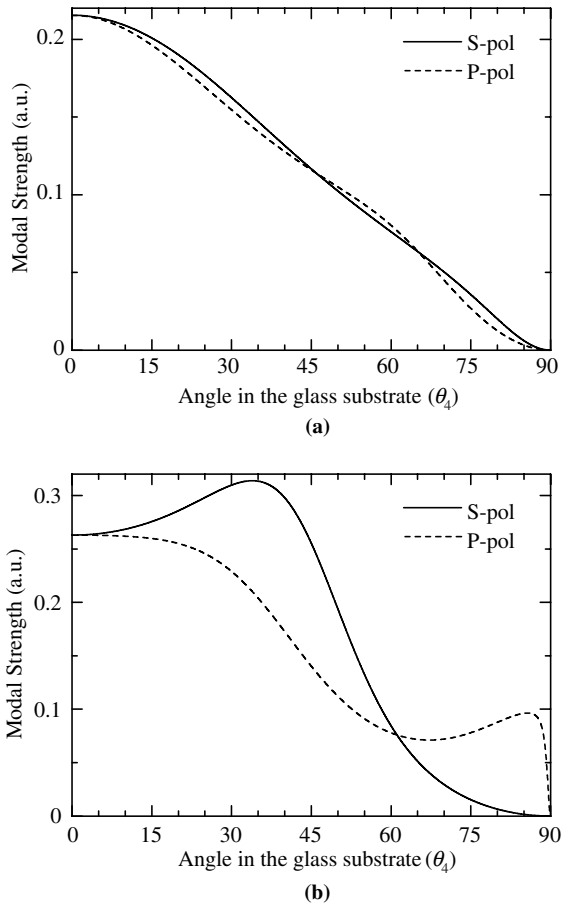

Fig. 5. Modal strength (intensity) of the radiation mode as a function of angle. The solid and dashed lines show modal strength of the S-polarized and P-polarized mode, respectively. The thickness of the Alq_3 and PVK layers is 80 and 40 nm, respectively. The thickness of the ITO layer is (a) 50 nm, (b) 130 nm.

mainly come from the insufficient resolution of the FDTD grid in defining the light cone with angle = 41.8°.

4. Conclusion

In summary, we have presented a theoretical analysis on light-extraction efficiency of the OLED using the FDTD and the mode-expansion method. An excellent agreement between the results of both methods was found, and thus confirmed the accuracy of our calculation. It has been found that even though the index contrast between the ITO layer and the glass substrate was as small as 0.5, more than 40% of emitted light power was trapped in the ITO layer.

In light of this analysis, we believe the FDTD method can be used as a powerful analytical tool for complex OLED designs since the method is applicable to virtually any type of structures, including one that is too complex to study by analytical methods. This makes the FDTD method very advantageous over analytic approaches. Furthermore, the FDTD method may be combined with the mode-expansion method to provide a novel and even more powerful analytical tool (that takes advantages of both methods) for the recently proposed microstructured OLED, for example, the OLED with photonic crystals [11,12].

Acknowledgements

This work is partly supported by a grant-in-aid for creative scientific research from the Ministry of Education, Culture, Sports, Science and Technology of Japan and the Kyoto University comprehensive innovation alliance.

References

[1] S.R. Forrest, Org. Electron. 4 (2003) 45.
[2] G. Gu, D.Z. Garbuzov, P.E. Burrows, S. Venkatesh, S.R. Forrest, Opt. Lett. 22 (1997) 396.
[3] M.-H. Lu, J.C. Sturm, J. Appl. Phys. 91 (2002) 595.
[4] J.S. Kim, P.K.H. Ho, N.C. Greenham, R.H. Friend, J. Appl. Phys. 88 (2000) 1073.
[5] M. Ikai, S. Tokito, Y. Sakamoto, T. Suzuki, Y. Taga, Appl. Phys. Lett. 79 (2001) 156.
[6] C. Adachi, M.A. Baldo, M.E. Thompson, S.R. Forrest, J. Appl. Phys. 90 (2001) 5048.
[7] K.S. Yee, IEEE Trans. Antennas Propagat. AP-14 (1966) 302.
[8] G. Mur, IEEE Trans. Electromagn. Compat. EMC-23 (1981) 377.
[9] E.A. Hinds, in: P.R. Berman (Ed.), Cavity Quantum Electrodynamics, Academic, New York, 1994.
[10] D. Meschede, W. Jhe, E.A. Hinds, Phys. Rev. A 41 (1990) 1587.
[11] M. Fujita, T. Ueno, T. Asano, S. Noda, H. Ohhata, T. Tsuji, H. Nakada, N. Shimoji, Electron. Lett. 39 (2003).
[12] Y.J. Lee, S.H. Kim, J. Huh, G.H. Kim, Y.H. Lee, S.H. Cho, Y.C. Kim, Y.R. Do, Appl. Phys. Lett. 82 (2003) 3779.